ACS APPLIED MATERIALS & INTERFACES

Research Article

www.acsami.org

Melt Spinning of Poly(lactic acid) and Hydroxyapatite Composite Fibers: Influence of the Filler Content on the Fiber Properties

Maria Persson,[†,‡] Gabriela S. Lorite,[‡] Sung-Woo Cho,[†] Juha Tuukkanen,[‡] and Mikael Skrifvars*[,†]

[†]School of Engineering, University of Borås, SE-501 90 Borås, Sweden

[‡]Department of Anatomy and Cell Biology, University of Oulu, FI-90014, Oulu, Finland

ABSTRACT: Composite fibers from poly(lactic acid) (PLA) and hydroxyapatite (HA) particles were prepared using melt spinning. Different loading concentrations of HA particles (i.e., 5, 10, 15, and 20 wt %) in the PLA fibers and solid-state draw ratios (SSDRs) were evaluated in order to investigate their influence on the fibers' morphology and thermal and mechanical properties. A scanning electron microscopy investigation indicated that the HA particles were homogeneously distributed in the PLA fibers. It was also revealed by atomic force microscopy and Fourier transform infrared spectroscopy that HA particles were located on the fiber surface, which is of importance for their intended application in biomedical textiles. Our results also suggest that the mechanical properties were independent of the loading concentration of the HA particles and that the SSDR played an important role in improving the mechanical properties of the composite fibers.

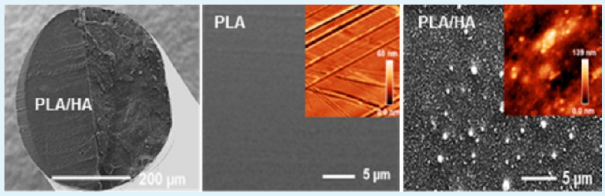

KEYWORDS: *poly(lactic acid), hydroxyapatite, melt spinning, fiber morphology, mechanical properties, thermal properties*

INTRODUCTION

Recent developments in tissue engineering have increased the need for scaffold materials that are designed to be bioactive so they can stimulate and promote cell attachment, proliferation, differentiation, and tissue regeneration.[1,2] Many mammalian cells are also anchorage-dependent, which requires the use of a scaffold design with a large surface area.[3,4] Other fundamental requirements of the scaffold material used in tissue regeneration are appropriate mechanical properties and biodegradability in concert with the native tissue to be engineered.[5] For these reasons, the selection of materials and fabrication technology of the scaffold has become a central issue for the success of tissue engineering.

Fabrication techniques that have been described for the design of a scaffold mainly include gas foaming,[6] freeze-drying,[7,8] solvent casting/particulate leaching,[9] phase separation,[3,10] and electrospinning.[11−14] Each technique has its advantages and disadvantages depending on the organ or target tissue under investigation. In particular, the use of textile technology to form a biodegradable scaffold provides several advantages for tissue-engineering applications. Fibers, which are the fundamental units of textile materials, are desirable as a scaffold matrix material because they provide a large surface area-to-volume ratio. In addition, textile technology has a high potential to provide ideal living conditions for cells because of the ability of fibers to be processed into a variety of shapes and sizes, thus achieving the desired mechanical and biological properties. Moreover, textile technology has also provided a breakthrough in the design of cartilage scaffolds for tissue engineering.[15] Economically, the treatment of injured/fractured bone is so far the most important surgical activity. However, to date, no textile structures have been used in this field probably because of limitations in obtaining appropriate fibers and modifying them for medical applications.

In this context, among various materials, poly(lactic acid) (PLA) is widely used as a synthetic polymeric material for tissue-engineering applications because of its biodegradability to nontoxic products, favorable mechanical properties, and great design flexibility. PLA is well suited for use as a fiber and has the advantage of U.S. Food and Drug Administration approval for clinical use.[16,17] However, the lack of cell recognition signals and its hydrophobic nature have limited its scope in tissue-engineering applications.[18,19] In order to overcome these disadvantages, a promising strategy has been to combine bioactive minerals as fillers inside the polymer matrix.[11−13,20]

One well-investigated bioactive mineral is hydroxyapatite (HA), which has been shown to mimic the natural bone mineral and stimulate bone growth. It is also known that a higher HA content in the composite leads to better composite bioactivity. The incorporation of HA in the PLA matrix has been well documented, and several investigators have demonstrated an increase in the mechanical properties of PLA/HA compared to the individual components.[3,11,13,21] Therefore, materials composed of PLA/HA are promising candidates as a scaffold material for the regeneration of bone tissue. In fact, natural bone matrix is an organic/inorganic composite material.[16] However, the incorporation of additives in fibers, even at low levels (i.e., <5 wt %), is challenging because it changes the spinnability, which can lead to spin-line

Received: September 24, 2012
Accepted: June 25, 2013
Published: June 25, 2013

failures.[22,23] Although the use of nanosize additives has been shown to overcome this problem, the addition of additives is known to restrict the drawability of the fibers, which decreases for higher concentrations of additives. The drawing stage is an important step in the fiber process because it causes disordered microfibrils to become more oriented in the direction of the fiber axis. The fiber drawing either can take place during melt extrusion, commonly referred to as the melt draw ratio (MDR), or undergo a drawing stage after solidification, which is known as solid-state drawing (SSD). An increased draw ratio leads to higher polymer chain orientation, which results in higher fiber tenacity.

Fiber spinning of PLA containing 0−50 wt % HA nanorods for use as reinforcement in PLA-based bone plates has been reported by Aydin et al.[24] They showed that the ultimate tensile strength decreased at any loading ratio compared to neat PLA, and because of the high brittleness of the fibers, they cannot be further processed into a textile structure, i.e., knitted, woven, or braided.

Our approach in this study was to develop a methodology to obtain novel bioactive melt-spun PLA/HA composite fibers with potential properties for use as orthopedic implant applications. Because melt spinning of filled polymer systems is a challenge, we especially studied and optimized the HA loading in the PLA matrix and the effect of SSD of the melt-spun fibers on the mechanical strength. The obtained fibers were further characterized by field-emission scanning electron microscopy (FE-SEM), atomic force microscopy (AFM), and Fourier transform infrared (FTIR) regarding the HA distribution and location in the fibers and by differential scanning calorimetry (DSC) and thermogravimetric analysis (TGA) regarding the thermal transitions, degree of crystallinity, and thermal stability. The goal of this original study was to develop a PLA composite fiber containing high loading concentrations of HA (i.e., 20 wt %) that still maintains the mechanical properties needed for further processing by weaving into textile structures.

EXPERIMENTAL SECTION

Materials. PLA (NatureWorks 6201D, fiber-grade resin) was provided by NatureWorks LLC, Minnetonka, MN. Commercially available HA particles (nanopowder, <200 nm) were purchased from Sigma-Aldrich. 1,4-Dioxane, laboratory reagent grade, and chloroform with a purity of ≥99.8% were purchased from Fisher Scientific, Loughborough, U.K. All materials and chemicals were used as received.

Preparation of Composite Materials and Melt Spinning. The composite PLA/HA fibers were prepared by the following procedure. In the first step, PLA/HA composite microspheres were prepared by the solvent evaporation method based on thermally induced phase separation, which enabled homogeneous HA dispersion in the PLA.[25] The HA particles were first dispersed in 1,4-dioxane and stirred for 4 h. The PLA pellets were then added and further stirred for 24 h. The resulting concentrations of HA were 5, 10, 15, and 20 wt % based on the polymer weight. Microspheres were then prepared by freezing droplets of the PLA/HA solution in liquid nitrogen. In order to remove the residual solvent, the microspheres were freeze-dried for at least 24 h at −50 °C. In a second step, the PLA/HA microspheres were extruded through a spinneret (D = 5.0 mm) with a melting temperature of 200 °C under a flow of argon using a laboratory-scale twin-screw extruder (DSM Research, Heerlen, The Netherlands). A screw rotation speed of 50 rpm and a dwell time of 5 min were selected to be optimal. Prior to processing, the PLA/HA microspheres were dried at 80 °C for 4 h. Granulates were thereafter made from the extruded material in a granulator (Axon AB, Sala, Sweden).

Finally, PLA/HA monofilament fibers were produced with a piston melt-spinning machine (Fourné Polymertechnik, Alfter, Germany) by a two-stage process, i.e., melt extrusion and hot drawing. The compounded PLA/HA granulates were extruded through a round-shape spinneret (D = 1.0 mm) with a melting temperature of 180 °C under an argon flow. The as-spun fibers were collected at a rate of 8.9 m/min, which corresponds to a MDR of 5.3. SSD was then carried out by passing the fibers around a heated godet (70 °C), then through a second heated godet (60 °C), and finally onto a take-up winder. The fibers were drawn to different SSDRs in the range of 3−5.

Intrinsic Viscosity Measurement. The molecular weight was measured by the viscosity method in a dilute polymer/chloroform solution (1.0 g/dL) using an Ubbelohde capillary viscometer (type 501 03/0, SCHOTT Instruments GmbH, Mainz, Germany) at 30 °C. The viscosity-average molecular weight, M_v, was calculated from the intrinsic viscosity, η, by using the Mark−Houwink−Sakurada equation given as

$$[\eta] = KM_v^{\ a} \tag{1}$$

where both K and a are specific constants for a given polymer, solvent, and temperature. K is 0.0131 and the exponent a is 0.759 for PLA solutions in chloroform at 30 °C, as reported in the literature.[26] The extent of the decrease in M_v was defined by the difference of M_v of the PLA/HA fiber before (M_{v1}) and after (M_{v2}) melt spinning, i.e.,

$$\text{extent of the decrease} = [(M_{v2} - M_{v1})/M_{v1}] \times 100\% \tag{2}$$

FTIR Spectroscopy. To investigate the chemical composition, FTIR spectra of the fibers were obtained using a Nicolet iS10 Fourier transform infrared spectrometer (Thermo Fisher Scientific Inc., Madison, WI) with the Zn/Se crystal attenuated total reflectance (ATR) mode. The spectra were taken as an average of 64 scans, with a wavelength resolution of 4 cm^{-1} and a spectral range of 4000−400 cm^{-1}, controlled by OMNIC analyzing software (Thermo Fisher Scientific Inc., Madison, WI). All spectra were analyzed using the software *OriginPro 8.6* (OriginLab Corp., Northampton, MA). In this case, the absorption intensities were analyzed using a Gaussian fit.

Gas Chromatography (GC). The presence of a residual solvent in the fibers after melt spinning was measured by a gas chromatograph−mass spectrometer (Hewlett-Packard G1800C, Agilent, Palo Alto, CA), equipped with a 30 m HP-5MS column (Hewlett-Packard). The injector and detector temperatures were 135 and 270 °C, respectively, and the initial column temperature was 45 °C, which was increased at a rate of 12 °C/min to 210 °C, at which point it was maintained for 1 min. Helium was used as the carrier gas (1.0 mL/min).

TGA. TGA data were obtained on a Q500 thermogravimetric analyzer (TA Instruments, New Castle, DE) to qualitatively confirm the thermal stability of the as-spun PLA/HA fibers. Samples of approximately 20 mg were heated at 10 °C/min from room temperature to 600 °C, under a nitrogen gas flow of 90 mL/min. Three replicates were scanned, and all obtained values were averaged.

DSC. Thermal transitions of the PLA/HA fibers were analyzed by using a Q1000 differential scanning calorimeter (TA Instruments, New Castle, DE) under a nitrogen atmosphere. The specimens containing 5−7 mg were mechanically sealed in aluminum pans. The DSC scans were performed within the temperature range of −20 to +250 °C at a heating rate of 20 °C/min. Three replicate specimens were scanned, and all obtained values were averaged. The midpoint glass transition (T_g), melting (T_m), and cold crystallization (T_c) temperatures from thermograms were recorded using TA Instruments software *Universal Analysis 2000*. All measurements were taken from the first scan. The degree of crystallinity (X_c^{DSC}) was estimated considering an ideal melting enthalpy of 93.7 J, according to the following equation:[27]

$$X_c^{\ DSC} = 100(\Delta H_m - \Delta H_c)/93.7 \tag{3}$$

Tensile Test. The mechanical properties of the fibers were evaluated using a Tinius-Olsen H10KT tensile machine (Tinius Olsen Inc., Horsham, Philidelphia, PA) with single bollard grips suitable for fibers. The tensile measurements were performed with a 250 N load cell at a crosshead speed of 12 mm/min and an initial grip separation

of 50 mm. The mean linear density was calculated from the weight of 5 m from the fibers. Prior to testing, the fibers were conditioned in a climate chamber at 23 °C and 50% relative humidity for 40 h. An average of 10 individual tensile determinations were reported for each sample together with the mean and standard deviation.

Optical Microscopy. The fiber diameter was measured using a Nikon optical microscope (model SMZ-800, Nikon Instruments Inc., Melville, NY) and *NIS-Element* image analysis software after calibration. The microscope was operated at 63× magnification to visualize the fibers. The result was reported as the average of five tests for each fiber.

FE-SEM. The surface morphology and cross section of the fibers were examined in a Zeiss ULTRA Plus field-emission scanning electron microscope (Oberkochen, Germany). Prior to analysis, the fractured cross-sectional specimens were fixed with a conducting carbon cement (Leit-C by Göcke) on the sample holder and dried under 0.1 mbar of vacuum pressure. To avoid charging, all samples were coated with a 5-nm-thick platinum layer using an Agarhigh resolution sputter coater (model 208HR) before placement in the FE-SEM chamber. The acceleration voltage was 5 kV.

AFM. Topography and phase images were acquired using a Nanoscope IV (Dimension 3100, Digital Instruments, Tonawanda, NY). AFM images were acquired in tapping mode in air using conical silicon tips with a typical tip radius of 10 nm and a tip length of ~20 μm (NSC14/AIBS MikroMash, Tallin, Estonia). The spring constant and resonance frequency were typically within the ranges of 1.8−12.5 N/m and 110−220 kHz, respectively. To evaluate the roughness of the surface, the root-mean-square (rms) roughness was determined over 10 × 10 μm^2 areas for each sample. All AFM images were analyzed using freely available software (*Gwyddion v. 2.9*).

Statistical Analysis. For mechanical and thermal properties, statistical analyses were carried out using a statistical software program, *JMP*, version 5 (SAS Institute Inc.). A Tukey−Kramer honestly significant difference (HSD) test, which performs a statistical means comparison for all pairs, was used at a significance level of 0.05.

RESULTS AND DISCUSSION

Fiber Morphology. Table 1 shows the calculated average diameters for all fibers produced. Diameter measurements showed that uniform as-spun fibers of about 380 μm were obtained, and the average diameter was unaffected by the addition of HA particles. Similarly, the SSD fibers produced were uniform, and the average diameter was not significantly affected by the addition of HA particles.

Table 1. Measurements of the Fiber Diameter by Optical Microscopy and rms by AFM Topography Image Analysis

	Diameter (μm)				rms (nm)
sample	as-spun	SSDR3	SSDR4	SSDR5	as-spun
PLA	384 ± 6	215 ± 2	185 ± 5	166 ± 5	10 ± 2
5% HA	381 ± 5	221 ± 8	187 ± 3	163 ± 5	17 ± 2
10% HA	386 ± 14	226 ± 8	190 ± 5	175 ± 4	19 ± 1
15% HA	384 ± 8	227 ± 4	190 ± 6	172 ± 8	23 ± 1
HA 20%	383 ± 10	226 ± 4	190 ± 7	177 ± 5	29 ± 2

In addition, the surface morphology of the fibers was investigated using SEM, as shown in Figure 1. SEM images not only reveal the presence of HA particles on the as-spun fibers' surface (seen as whitish features) but also clearly show that the density of the HA particles (particles/area) increases with increasing loading concentration. SEM images of the fibers drawn to different SSDRs also demonstrated that the HA particles were still present on the fibers' surface (data not shown).

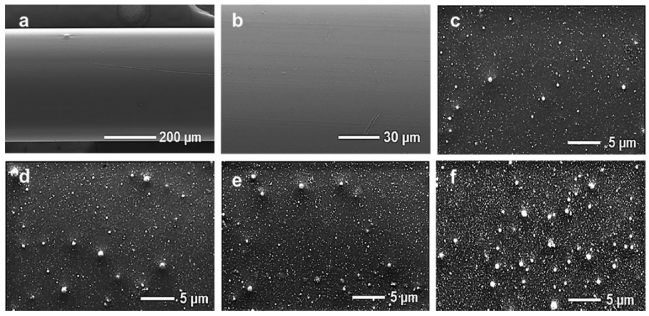

Figure 1. FE-SEM images of the surface of as-spun fiber/neat PLA (a and b), 5 wt % HA/PLA (c), 10 wt % HA/PLA (d), 15 wt % HA/PLA (e), and 20 wt % HA/PLA (f).

In order to understand the distribution of the HA particles on the fibers' surface, different areas of both pure PLA and PLA/HA fibers were scanned by AFM. Although there were some limitations related to sample preparation and surface imaging difficulties due to the curvature of the fibers, topography and phase images were successfully acquired, as shown in Figure 2. As expected from the SEM images, AFM topography images show different morphologies for pure PLA (Figure 2a) and composite fibers (Figure 2b,e). PLA fibers present an irregular surface, while the PLA/HA fibers present a granular morphology. In addition, the roughness (rms) was evaluated for each sample, as shown in Table 1. Our data clearly show that the rms value increases with increasing loading concentration of the HA particles. This result is not just due to a higher number of HA particles on the fiber surface but also due to the presence of agglomerates.

HA agglomerates on the fibers' surface can be observed in both SEM and AFM images. From SEM images, it is evident that the amount of agglomerates increases for higher loading concentrations (Figure 1f). Cross sections from the AFM topography images show that the agglomerates vary considerably in size in both their diameter and height (400−900 and 60−120 nm, respectively). However, single particles with diameters between 120 and 200 nm and heights between 8 and 25 nm also can be observed (Figure 2d). These analyses also indicate that HA particles or agglomerates are partially inside the PLA net but still exposed on the surface. In addition, HA also formed small agglomerates in the fiber bulk at all loading concentrations (Figure 3). The aggregation occurs because PLA has no chemical affinity for the HA particles. In order to overcome the aggregation effect, surfactants could be used for uniform dispersion of the polar HA particles into the nonpolar PLA matrix. However, the small agglomerate size of the particles gives rise to an increase in the roughness of the fibers' surface. The authors of some studies[28,29] have proposed that an increase in the surface roughness could enhance cell adhesion because substrates with more topographical features will expose more surface area for possible interactions with both proteins and cells. In contrast, other authors concluded that the roughness is not a determinant feature in cell adhesion[30] or have even observed that the adhesion force falls as the surface roughness increases.[31] Therefore, more research on this topic needs to be undertaken before the association between the surface roughness of the fiber and cell adhesion can be more clearly understood. In addition to topography images, phase images were acquired using AFM. It is know that a phase image records the phase shift signal in tapping-mode AFM. The contrast in the phase image is often interpreted as variations in

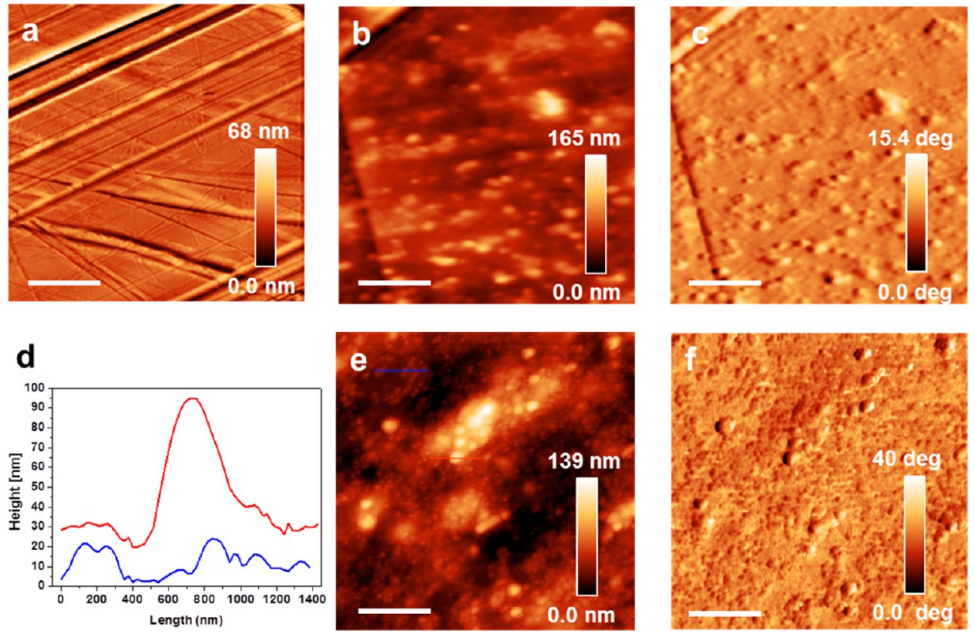

Figure 2. Topography (a, b, and e) and phase (c and f) AFM images for neat PLA (a), 5 wt % HA/PLA (b and c), and 20 wt % HA/PLA (e and f). Corresponding profiles for particles (blue) and agglomerates (red) for 20 wt % HA/PLA fibers (e) are shown in part d. The scale bar is 2 μm in all images.

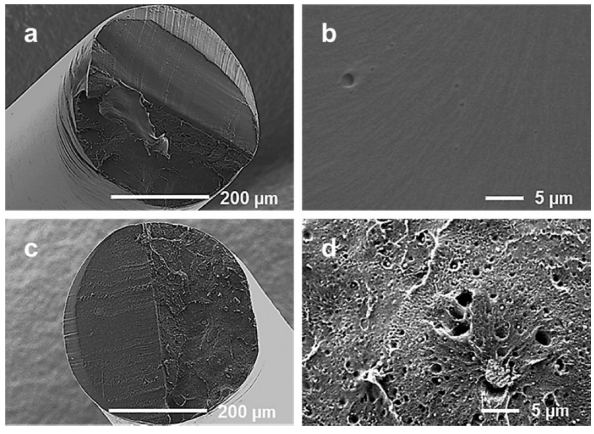

Figure 3. FE-SEM images of the cross section of as-spun fiber/neat PLA (a and b) and 20 wt % HA/PLA (c and d).

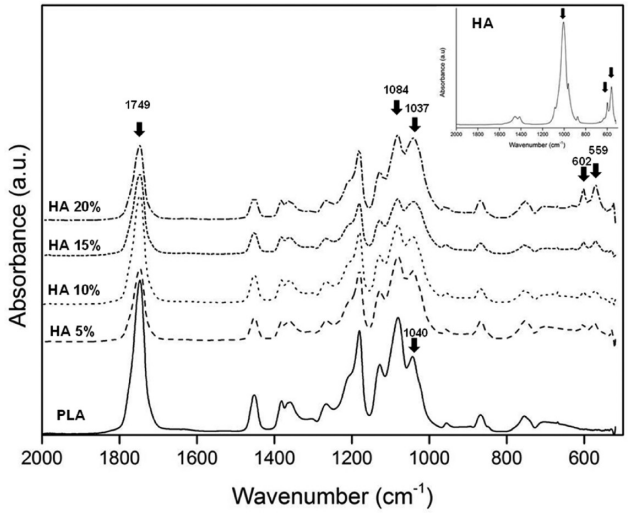

Figure 4. FTIR spectra of as-spun neat PLA and PLA/HA composite fibers with different loading concentrations. Inset: FTIR spectra of HA particles.

the local mechanical properties or surface viscoelasticity. Our data show homogeneous phase images, indicating that the presence of HA particles or agglomerates does not affect the local mechanical properties (Figure 2c,f).

Chemical Composition. Figure 4 shows FTIR spectra for neat PLA fibers, HA particles, and PLA/HA fibers. The same IR bands were observed for all PLA/HA fibers except for the peak intensity. The bands at 1005 cm^{-1} are attributed to the $\nu_3(PO_4^{3-})$, and those at 602 and 559 cm^{-1} are attributed to the $\nu_4(PO_4^{3-})$. These bands are clearly attributed to pure HA because they are not present in the neat PLA spectrum (arrows in Figure 3, inset). Three characteristic bands can be identified in the spectrum of neat PLA at 1040, 1084, and 1749 cm^{-1}, which are assigned to C−CH_3, C−O−C, and C═O stretching, respectively. Therefore, the final spectra for PLA/HA fibers are clearly a combination of individual spectra from neat PLA and HA particles as predicted.

A comparison of the PLA/HA fibers at low (i.e., 5 wt %) and higher (i.e., 20 wt %) loading concentrations showed that the bands at 602 and 559 cm^{-1} increased 60% and 82%, respectively. This result provides chemical evidence for the presence of HA particles on the fibers' surfaces because the penetration depth into the sample of the IR-ATR technique is typically between 0.5 and 5 μm. Moreover, the observed increase of the absorption intensity with increasing HA loading concentration is consistent with the SEM and AFM images (Figures 1 and 2).

In addition, the intensity of the band at 1040 cm^{-1} increased by 82% from the low (i.e., 5 wt %) to higher (i.e., 20 wt %) HA loading concentration. Furthermore, the ratio between the C−O−C (1084 cm^{-1}) and C−CH_3 (1040 cm^{-1}) stretching was observed to decrease in the composite fibers compared with neat PLA fibers. These results altogether indicate that the band at 1040 cm^{-1} from neat PLA is convoluted with the broad band

dx.doi.org/10.1021/am401895f | ACS Appl. Mater. Interfaces 2013, 5, 6864−6872

(~60 cm^{-1}) at 1005 cm^{-1} from HA, which suggests that HA interferes with the vibrational properties of PLA.

The spectral resolution of the band widths for neat PLA and HA particles shows that no peak shift was observed. This suggests that HA does not cause internal stress in PLA. Moreover, the SSD fibers were also investigated with FTIR (data not shown), which showed that HA particles were still present toward the surface and the intensity of the peaks for PO_4^{3-} was not affected by the SSDR.

Thermal Degradation. Thermal degradation during the fiber preparation was evaluated by measuring the intrinsic viscosities both before and after the compounding and melt-spinning process. Our results clearly show that a low material degradation occurred during the compounding process but decreased sharply during the melt-spinning process (Table 2). The extent of decrease during the compounding process was about 1.9%, and during the melt-spinning process, it was 89.7%.

Table 2. Intrinsic Viscosity of PLA and Its Decrease during Fiber Preparation

sample	intrinsic viscosity (η)	extent of decrease (%)
neat PLA	1.07	
after compounding[a]	1.05	1.9
after melt spinning[b]	0.11	89.7

[a]After 5 min of processing at 200 °C. [b]After 60 min of processing at 180 °C.

In previous work,[32] it was demonstrated that the thermal degradation of PLA is directly dependent on the time in the molten state and the initial molecular weight of the polymer. In addition, it was shown that the extent of decrease in the viscosity-average molecular weight for PLA quality identical with that used in this study dropped about 16% after 90 min of processing at 180 °C during the melt-spinning process. Therefore, our results suggest that the two consecutive thermal processing steps (i.e., compounding and melt spinning) caused molecular degradation of PLA to a high extent. In order to reduce the thermal degradation, PLA should only be heated above its melting temperature once.

However, it was necessary to first process the material in the compounder before melt spinning in order to reduce the volume of the material because the microspheres contained air and to thermally embed the HA particles in PLA. When the microspheres were directly fed into the piston machine, the HA particles separated from the PLA phase because of a lack of adhesion between the hydrophilic HA particles and the hydrophobic PLA matrix. As a result, the thermal degradation of the material was accelerated and fibers of good quality could not be obtained.

Previous studies have also suggested that low-molecular-weight impurities and humidity can cause molecular degradation of PLA.[33,34] Therefore, the possible presence of residual solvent dioxane was investigated using GC analysis. Dioxane was not detected in the PLA/HA materials, which indicates that the dioxane removal conditions were optimized in this study. The dehumidification conditions were also optimized because no hydrolysis reactions occurred during the fiber preparation, as confirmed by FTIR.

Thermal Decomposition and Stability. Figure 5 shows the weight loss (%) and derivative weight loss curves of the PLA, PLA/HA fibers, and HA particles. TGA plots of the fibers indicate that decomposition of the samples starts at around 300 °C and is complete around 380 °C. The HA particles did not undergo thermal decomposition within the range of temperatures tested. This result provides evidence that the amount of HA particles used plays an important role in the thermal stability of the fibers. As shown in Table 3, the thermal stability of the various samples was established by measuring various characteristic temperatures at which 5 (T_5) and 50% (T_{50}) of the initial weight were lost due to volatilization. Thermal stability enhancement takes place at a low loading concentration (i.e., 5 wt %) of HA, while at higher concentrations of HA in the PLA fibers, the thermal stability decreases gradually compared with neat PLA fibers. However, the decrease in the thermal stability at higher loading concentrations (≥10 wt %) was not statistically significant compared with that of neat PLA. In addition, the thermal degradation of the fibers was almost invariable, and decomposition occurs at approximately the same temperature. The slight increase in T_{50} at 20 wt % HA compared with 15 wt % HA can be attributed to restriction of the PLA polymer chain mobility due to the high loading concentration of the additive.

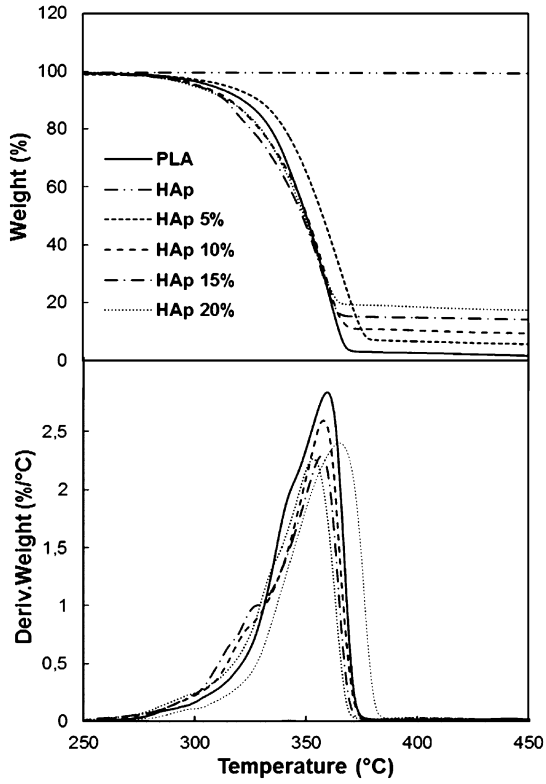

Figure 5. TGA of as-spun PLA/HA composite fibers. Mass loss (%) versus temperature (a) and first derivative mass loss (%/°C) versus temperature (b).

Table 3. Characteristic Temperatures of the Thermal Decomposition of As-Spun PLA/HA Composite Fibers

sample	T_5[a] (°C)	T_{50}[a] (°C)	T_p (°C)
PLA	308.7 ± 2.7	351.9 ± 2.1	362.0 ± 2.0
5% HA	314.5 ± 3.0	358.1 ± 1.1	365.5 ± 1.6
10% HA	303.2 ± 2.6	351.3 ± 2.0	358.9 ± 1.7
15% HA	301.4 ± 1.2	349.4 ± 1.1	357.2 ± 0.9
20% HA	300.0 ± 2.6	351.0 ± 2.4	356.1 ± 3.1

[a]T_x = temperature at which x % of the initial mass is lost.

dx.doi.org/10.1021/am401895f | ACS Appl. Mater. Interfaces 2013, 5, 6864−6872

The peak temperature (T_p) in the first derivate, which is related to the highest decomposition rate, was observed at 362.0 °C for neat PLA fibers. PLA fibers containing 5 wt % HA exhibited a slightly higher T_p value (i.e., 3.5 °C higher), resulting in a 1% increase in the thermal stability. At higher contents of HA, the T_p values were observed to shift to a lower temperature (i.e., decreases with a mean value of 4.6 °C). The temperature decrease at the higher loading concentrations, at both T_5 and T_p, could be attributed to the observed aggregation of HA particles in the PLA fibers. A recent review[35] has suggested that, as high amounts of nanosized filler aggregates are formed, the structure may shift from nanocomposite to microcomposite. Thus, the shielding effect of the nanosized particles is lessened. In addition, Chen et al.[36] reported high loading concentrations of HA particles that have been well dispersed in the polymer matrix of poly(3-hydroxybutyrate-*co*-3-hydroxyvalerate) also lower the onset degradation temperature (i.e., T_5). Similar results were found by Jeong et al.[13] Therefore, our results indicate that high loading concentrations of HA particles in the polymer matrix catalyze the decomposition at the initial stage, but at lower loading concentrations (<5 wt %), an improvement of the thermal stability, at all temperature ranges, took place.

Thermal Properties. The obtained data from the DSC curves of as-spun fibers as well as for SSD fibers are listed in Table 4. The as-spun fibers showed a clear T_g, around 58.2–63.8 °C. The T_g was observed to initially decrease with increasing loading concentration, reaching a minimum of 56.1 °C at 15 wt % HA. However, as the weight percent of HA increased from 15 to 20 wt %, T_g increased to 62.6 °C. This phenomenon has been explained by Wilberforce et al.[37] These authors concluded that T_g is highly dependent on the surface area of the HA particles and the number of particles per unit volume in the composites. In addition, a higher loading concentration of HA particles leads to an increase in the interfacial area, which increases the flexibility of the polymer chain and thus decreases T_g. Thus, the observed increase in T_g at 20 wt % HA particles can be attributed to the relatively high agglomeration of particles, which lowers the polymer chain mobility. Therefore, more energy is needed to mobilize the polymer chains, resulting in a higher T_g. Furthermore, a cold crystallization peak (T_c) was observed in the range of 109.1–123.7 °C for the as-spun fibers, which dropped with increasing loading concentration of HA particles. According to the literature,[37−39] this effect is due to the presence of HA particles, which act as nucleating agents for the formation of PLA crystals at lower temperatures. The degree of crystallinity for the as-spun fibers was in the range of 4.9–14.3% (Figure 6).

Table 4. Thermal Properties of As-Spun and SSD PLA/HA Composite Fibers[a]

sample	SSDR	T_g (°C)	T_c (°C)	T_m (°C)
PLA	as-spun	63.8 ± 0.0	123.7 ± 0.6	168.4 ± 0.1
	3	70.7 ± 0.7	81.7 ± 0.2	168.6 ± 0.9
	4	71.5 ± 0.7	81.7 ± 1.0	168.0 ± 0.1
	5	73.0 ± 0.5	81.3 ± 0.1	167.8 ± 0.6
5% HA	as-spun	62.6 ± 0.9	113.5 ± 0.3	168.3 ± 0.2
	3	65.6 ± 0.9	80.7 ± 0.3	167.0 ± 0.3
	4	71.8 ± 0.2	80.7 ± 0.2	166.9 ± 0.3
	5	71.3 ± 0.9	80.6 ± 0.2	166.8 ± 0.5
10% HA	as-spun	58.2 ± 0.3	112.0 ± 1.0	167.9 ± 0.3
	3	68.2 ± 0.4	80.5 ± 0.5	167.0 ± 0.6
	4	71.1 ± 0.9	80.3 ± 0.3	166.7 ± 0.0
	5	71.8 ± 0.6	80.2 ± 0.8	166.4 ± 0.4
15% HA	as-spun	56.1 ± 0.2	109.1 ± 0.5	167.3 ± 0.1
	3	69.8 ± 0.6	80.4 ± 0.6	166.9 ± 0.3
	4	69.9 ± 0.8	79.2 ± 0.3	166.1 ± 0.2
	5	70.7 ± 0.8	79.7 ± 0.3	166.1 ± 0.1
20% HA	as-spun	62.6 ± 0.4	109.8 ± 1.2	167.8 ± 0.5
	3	70.3 ± 0.7	79.2 ± 0.4	166.7 ± 0.9
	4	71.5 ± 0.8	80.6 ± 0.5	166.6 ± 0.5
	5	72.3 ± 0.4	81.4 ± 0.6	166.2 ± 0.2

[a] T_g = glass transition temperature. T_c = cold crystallization temperature. T_m = melting temperature.

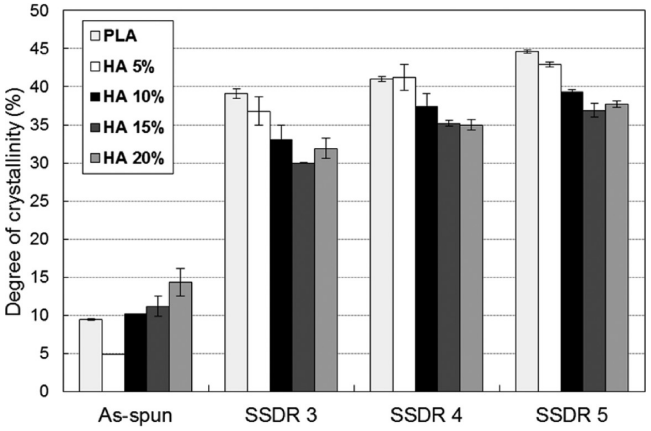

Figure 6. Degree of crystallinity of PLA/HA fibers with respect to the SSDR obtained from the DSC thermograms.

At low loading concentrations of HA (i.e., 5 wt %), the crystallinity decreased compared with neat PLA; however, at higher loading concentrations, an increase was observed. This result indicates that HA particles enhance the crystallinity in as-spun fibers and act as nucleation sites for the crystallization of PLA at higher loading concentrations (i.e., >10 wt %). Therefore, the addition of HA particles in the as-spun fibers had no significant effect on the melting temperature (T_m), but the slight decrease indicates that the crystallite size was less stable.

As shown in Figure 6, SSD had a significant influence on the degree of crystallinity of all fibers, which increases with increasing SSDR. In contrast to the as-spun fibers, the crystallinity decreases with increasing loading concentrations of HA particles, with the exception of the loading concentration of 20 wt %, where the crystallinity increases slightly. These results, therefore, suggest that HA particles prevent the macromolecules from being fully oriented along the fiber axis during the SSD process.

A significant effect of the SSD process is the modification of T_m, which was observed to decrease with increasing SSDR. This occurred for PLA/HA fibers irrespective of the loading concentration of HA particles as well as for neat PLA fibers. Therefore, it is likely that the modification of T_m correlates with the crystalline phase. Moreover, it was observed that T_c shifted to a lower temperature, in the range of 79.2–81.7 °C, after SSD compared with as-spun fibers. This result indicates that none of the fibers in this study was sufficiently crystallized.[40] T_g increased with increasing SSDR for all fibers because of the higher crystallinity, which decreases the molecular mobility. However, it should be noted that T_g was not readily determined

dx.doi.org/10.1021/am401895f | ACS Appl. Mater. Interfaces 2013, 5, 6864−6872

for the SSD fibers, and these data therefore need to be interpreted with caution. As an example, the DSC thermograms of PLA fibers containing 15 wt % HA particles are shown in Figure 7. In this figure, T_g seems to appear in two steps, with a

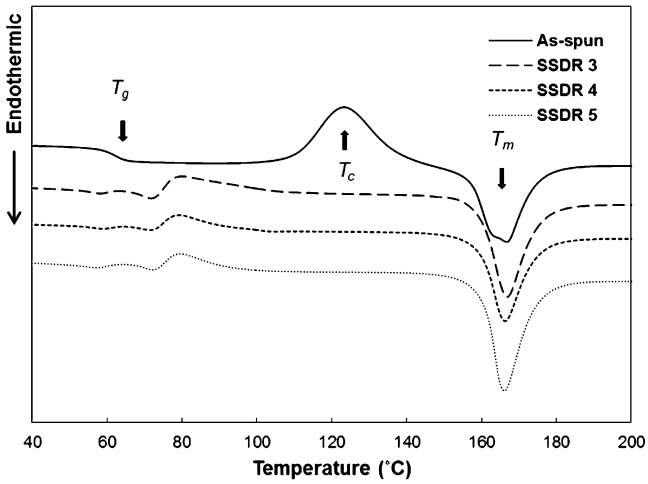

Figure 7. DSC thermograms obtained for PLA containing 15 wt % HA particle fibers with respect to the SSDR (first heating scan).

small exothermic peak between them. This effect can be due to the stress built into the fibers as a result of SSD because it was not detected in the second scan, when the fibers had been cooled to a temperature below its T_g.

Mechanical Properties. The mechanical properties of the fibers are shown in Figure 8, and Table 5 provides a summary of the results. The tenacity and elongation at break for the as-spun fibers were in the ranges of 2.6−3.1 cN/Tex and 15.3−23.3%, respectively, and there were no significant differences ($P < 0.05$). The initial modulus of the as-spun fibers was observed to decrease with an increase in the HA content, although the differences were small and mostly insignificant.

However, the SSDR of the fibers significantly improves the tenacity, which increases with increasing SSDR. Tenacity showed a maximum of 16.7 cN/Tex for PLA fibers containing 10 wt % HA at SSDR5. In comparison with the other fibers with SSDR5, there was only a significant difference for the PLA fibers containing 20 wt % HA ($P < 0.05$). The initial modulus increased with increasing SSDR for neat PLA fibers and for PLA fibers containing 5 wt % HA. At higher loading concentrations of HA particles (i.e., >10 wt %), the initial modulus reached its maximum at SSDR4. Elongation at break increased drastically from as-spun fibers compared with fibers at SSDR3 (Figure 8c). At higher SSDRs (i.e., 4 and 5), the elongation at break decreased. Tukey−Kramer's HSD test showed that the result from elongation at break of fibers with the same SSDR was not statistically significant. In general, this result indicates that the mechanical properties were basically independent of the loading concentration of HA particles but that the SSDR played an important role in improving the mechanical properties of the fibers. This result has not previously been described. Jeong et al.[13] showed that the tensile strength increased with an increasing amount of HA particles in the electrospun PLA/HA composite scaffolds. Similar observations were reported by Sui et al.[12] In order to obtain this improvement of the mechanical properties, a strong interaction between the matrix and the filler is required.[9] It is also hypothesized that the distribution of the filler should be

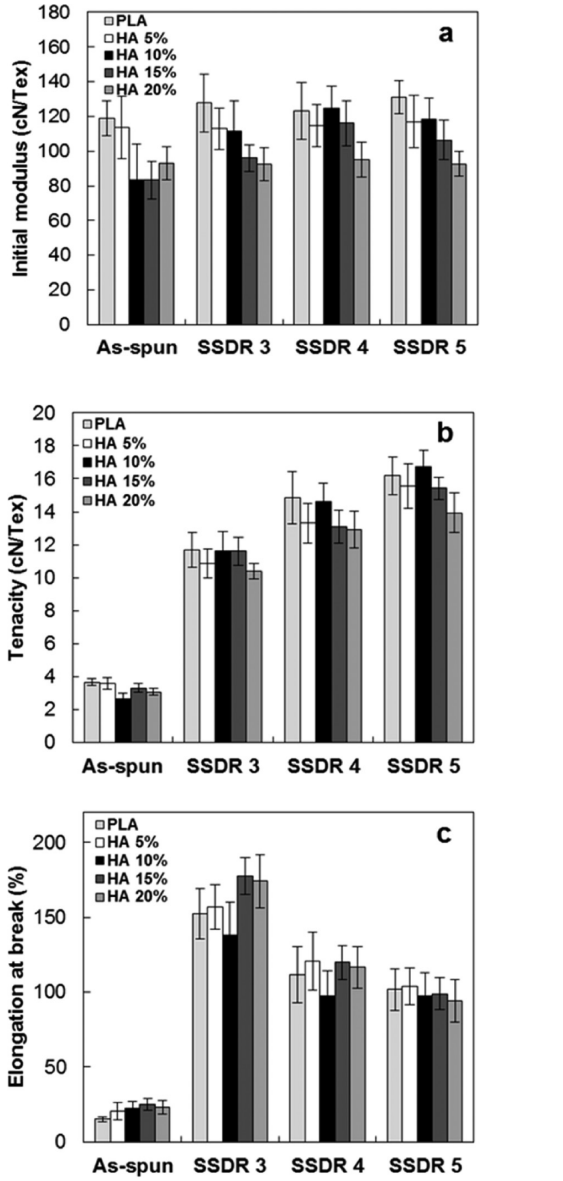

Figure 8. Initial modulus (a), tenacity (b), and elongation at break (c) of PLA/HA composite fibers with respect to the SSDR.

homogeneous. Aydin et al.[24] reinforced PLA fibers with HA nanorods. They showed that the tensile strength decreased dramatically at any loading concentration compared with neat PLA, although HA nanorod particles were evenly distributed within the polymer bulk. Our results demonstrated that the HA particles in the PLA fibers did not affect the mechanical properties significantly compared with neat PLA fibers, even when agglomerations of HA were observed. To improve the interaction between the HA particles and PLA, HA particles should be surface grafted with lactic acid; thus, the mechanical properties can be expected to increase.[24,41]

CONCLUSIONS

PLA/HA composite fibers with various loading concentrations of HA particles were successfully prepared using melt spinning. Morphological investigations of the incorporation clearly showed that HA particles were homogeneously distributed in the melt-spun PLA fibers. It was also revealed that the particles were located at the surface, which is important in order to

Table 5. Mechanical Properties of PLA/HA Composite Fibers with Respect to the SSDR[a]

sample	SSDR	Tex	initial modulus (cN/Tex)	tenacity (cN/Tex)	elongation at break (%)
PLA	as-spun	149.6	119.0 ± 10.1 ab[b]	3.7 ± 0.2 i	15.3 ± 1.7 h
	3	49.8	127.8 ± 16.7 a	11.7 ± 1.1 gh	152.4 ± 16.6 bc
	4	41.6	123.1 ± 13.5 ab	14.9 ± 1.6 bcd	111.6 ± 18.5 efg
	5	38.6	130.9 ± 9.5 a	16.2 ± 1.1 ab	101.7 ± 16.7 efg
5% HA	as-spun	157.0	113.6 ± 17.8 abcde	3.5 ± 0.4 i	20.6 ± 5.7 h
	3	52.6	113.0 ± 11.9 abcdef	10.9 ± 0.9 h	157.0 ± 15.1 abc
	4	46.2	114.8 ± 12.1 abcd	13.3 ± 1.2 ef	120.0 ± 11.3 de
	5	41.2	116.8 ± 15.1 abc	15.6 ± 1.3 abc	103.8 ± 12.3 efg
10% HA	as-spun	162.8	83.6 ± 20.7 g	2.6 ± 0.3 i	22.2 ± 4.6 h
	3	56.0	111.4 ± 17.5 abcdef	11.6 ± 1.2 h	138.1 ± 21.8 cd
	4	47.4	124.6 ± 13.0 ab	14.6 ± 1.1 cde	97.4 ± 17.0 fg
	5	42.8	118.6 ± 12.1 ab	16.7 ± 1.0 a	97.3 ± 15.7 fg
15% HA	as-spun	167.8	83.4 ± 10.8 g	3.3 ± 0.3 i	25.0 ± 3.9 h
	3	56.0	96.0 ± 7.7 cdefg	11.7 ± 0.8 gh	177.5 ± 12.1 a
	4	47.8	116.0 ± 13.1 abc	13.1 ± 1.0 fg	120.0 ± 11.3 de
	5	43.4	106.4 ± 11.3 bcdef	15.4 ± 0.7 abcd	99.0 ± 10.9 efg
20% HA	as-spun	172.4	93.0 ± 9.6 efg	3.1 ± 0.2 i	23.2 ± 4.3 h
	3	58.4	92.5 ± 9.5 fg	10.4 ± 0.5 h	174.1 ± 17.9 ab
	4	48.4	95.1 ± 10.2 defg	12.9 ± 1.1 fg	116.6 ± 14.2 def
	5	44.6	92.6 ± 7.0 fg	13.9 ± 1.2 def	94.2 ± 14.2 g

[a]The results are given with the average value, standard deviation, and significance letters. [b]The values having the same letters are not significantly different. Statistics was carried out using Tukey–Kramer's HSD test at a significance level of 0.05.

maintain the bioactive effect of the HA particles. In addition, our results revealed an increase in rms with increased loading concentrations of HA particles, which can be due to the formation of the small HA agglomerates (<900 nm in diameter) observed for all loading concentrations. Our results also provide substantial evidence that the mechanical properties were independent of the loading concentration of HA particles and also that the SSDR played an important role in improving these properties. The results also indicated that thermal degradation occurred during the melt spinning, which could be limited by heating the polymer only once. This could alter the later in vivo and in vitro degradation behavior of the final product. To investigate this aspect, long-term experiments are necessary to further determine the fibers' usefulness in orthopedic applications.

In this original article, we provide experimental evidence that it is possible to melt-spin composite fibers from blends composed of HA particles and the PLA matrix even at high HA loading concentrations (i.e., 20 wt %). The fabricated melt-spun HA/PLA composite fibers possessed adequate mechanical strength and thermal stability to be useful in textile processes such as weaving. Because the fibers have high bioactive HA particles on the surface, they could be potentially suitable in bone-tissue-engineering textile applications.

AUTHOR INFORMATION

Corresponding Author

*Tel.: +46 33 435 4497. Fax: +46 33 435 4008. E-mail: Mikael.Skrifvars@hb.se.

Notes

The authors declare no competing financial interest.

ACKNOWLEDGMENTS

The authors thank M.Sc. (Tech) Jarkko Puustinen for his kind support and Microelectronics and Material Physics Laboratories, University of Oulu, for the AFM facilities. This work was funded in part through a grant from the Bo Rydin Foundation, SCA, Sweden, Gunilla Edlinds Foundation, SEB AB, Sweden, and the School of Engineering, University of Borås, Sweden. Part of this work has been performed in the project Scaffolds for Tissue Engineering, which belongs to the MATERA Era-Net program and is financed by the national agencies TEKES and MIUR.

REFERENCES

(1) Armentano, I.; Dottori, M.; Fortunati, E.; Mattioli, S.; Kenny, J. *Polym. Degrad. Stab.* **2010**, *95*, 2126–2146.
(2) Jagur-Grodzinski, J. *Polym. Adv. Technol.* **2006**, *17*, 395–418.
(3) Wei, G.; Ma, P. X. *Biomaterials* **2004**, *25*, 4749–4757.
(4) Ma, P. X. In *Encyclopedia of Polymer Science and Technology*; John Wiley & Sons, Inc.: New York, 2002; Vol. *12*, pp 262–291.
(5) Shoichet, M. S. *Macromolecules* **2009**, *43*, 581–591.
(6) Montjovent, M. O.; Mathieu, L.; Hinz, B.; Applegate, L. L.; Bourban, P. E.; Zambelli, P. Y.; Månson, J. A.; Pioletti, D. P. *Tissue Eng.* **2005**, *11*, 1640–1649.
(7) Roether, J.; Gough, J.; Boccaccini, A. R.; Hench, L.; Maquet, V.; Jérôme, R. *J. Mater. Sci., Mater. Med.* **2002**, *13*, 1207–1214.
(8) Deville, S.; Saiz, E.; Tomsia, A. P. *Biomaterials* **2006**, *27*, 5480–5489.
(9) Kothapalli, C. R.; Shaw, M. T.; Wei, M. *Acta Biomater.* **2005**, *1*, 653–662.
(10) Maquet, V.; Boccaccini, A. R.; Pravata, L.; Notingher, I.; Jérôme, R. *Biomaterials* **2004**, *25*, 4185–4194.
(11) Kim, H. W.; Lee, H. H.; Knowles, J. *J. Biomed. Mater. Res., Part A* **2006**, *79*, 643–649.
(12) Sui, G.; Yang, X.; Mei, F.; Hu, X.; Chen, G.; Deng, X.; Ryu, S. *J. Biomed. Mater. Res., Part A* **2007**, *82*, 445–454.
(13) Jeong, S. I.; Ko, E. K.; Yum, J.; Jung, C. H.; Lee, Y. M.; Shin, H. *Macromol. Biosci.* **2008**, *8*, 328–338.
(14) Zhou, C.; Shi, Q.; Guo, W.; Terrell, L.; Qureshi, A.; Hayes, D. J.; Wu, Q. *ACS Appl. Mater. Interfaces* **2013**, *5*, 3847–3854.
(15) Moutos, F. T.; Freed, L. E.; Guilak, F. *Nat. Mater.* **2007**, *6*, 162–167.
(16) Liu, X.; Ma, P. X. *Ann. Biomed. Eng.* **2004**, *32*, 477–486.
(17) Gupta, B.; Revagade, N.; Hilborn, J. *Prog. Polym. Sci.* **2007**, *32*, 455–482.
(18) Chen, Y.; Mak, A. F. T.; Wang, M.; Li, J.; Wong, M. *J. Mater. Sci., Mater. Med.* **2008**, *19*, 2261–2268.
(19) Liu, X.; Won, Y.; Ma, P. X. *J. Biomed. Mater. Res., Part A* **2005**, *74*, 84–91.
(20) Rizzi, S. C.; Heath, D.; Coombes, A. G. A.; Bock, N.; Textor, M.; Downes, S. *J. Biomed. Mater. Res., Part A* **2001**, *55*, 475–486.
(21) Bleach, N.; Tanner, K.; Kellomäki, M.; Törmälä, P. *J. Mater. Sci., Mater. Med.* **2001**, *12*, 911–915.
(22) Lee, S. H.; Youn, J. R. *J. Appl. Polym. Sci.* **2008**, *109*, 1221–1231.

(23) Solarski, S.; Ferreira, M.; Devaux, E. *Polym. Degrad. Stab.* **2008**, *93*, 707−713.
(24) Aydin, E.; Planell, J. A.; Hasirci, V. *J. Mater. Sci., Mater. Med.* **2011**, 1−15.
(25) Lee, K. Y.; Blaker, J. J.; Bismarck, A. *Compos. Sci. Technol.* **2009**, *69*, 2724−2733.
(26) Dorgan, J. R.; Janzen, J.; Knauss, D. M.; Hait, S. B.; Limoges, B. R.; Hutchinson, M. H. *J. Polym. Sci., Part B: Polym. Phys.* **2005**, *43*, 3100−3111.
(27) Garlotta, D. *J. Polym. Environ.* **2001**, *9*, 63−84.
(28) Cui, Y.; Liu, Y.; Cui, Y.; Jing, X.; Zhang, P.; Chen, X. *Acta Biomater.* **2009**, *5*, 2680−2692.
(29) Yanagida, H.; Okada, M.; Masuda, M.; Ueki, M.; Narama, I.; Kitao, S.; Koyama, Y.; Furuzono, T.; Takakuda, K. *J. Biosci. Bioeng.* **2009**, *108*, 235−243.
(30) Lorite, G. S.; Janissen, R.; Clerici, J. H.; Rodrigues, C. M.; Tomaz, J. P.; Mizaikoff, B.; Kranz, C.; de Souza, A. A.; Cotta, M. A. Submitted in 2013.
(31) Liu, D.; Martin, J.; Burnham, N. *Appl. Phys. Lett.* **2007**, *91*, 043107−043107−3.
(32) Persson, M.; Cho, S.; Skrifvars, M. *J. Mater. Sci.* **2013**, *48*, 3055−3066.
(33) Taubner, V.; Shishoo, R. *J. Appl. Polym. Sci.* **2001**, *79*, 2128−2135.
(34) Lim, L. T.; Auras, R.; Rubino, M. *Prog. Polym. Sci.* **2008**, *33*, 820−852.
(35) Bikiaris, D. *Thermochim. Acta* **2011**, *523*, 25−45.
(36) Chen, D.; Tang, C.; Chan, K.; Tsui, C.; Yu, P. H. F.; Leung, M. C. P.; Uskokovic, P. *Compos. Sci. Technol.* **2007**, *67*, 1617−1626.
(37) Wilberforce, S. I. J.; Finlayson, C. E.; Best, S. M.; Cameron, R. E. *Polymer* **2011**, *52*, 2883−2890.
(38) Wei, J.; Sun, J.; Wang, H.; Chen, X.; Jing, X. *Chin. J. Polym. Sci.* **2010**, *28*, 499−507.
(39) Wilberforce, S. I. J.; Finlayson, C. E.; Best, S. M.; Cameron, R. E. *Acta Biomater.* **2011**, *7*, 2176−2184.
(40) Kim, M. S.; Kim, J. C.; Kim, Y. H. *Polym. Adv. Technol.* **2008**, *19*, 748−755.
(41) Hong, Z.; Zhang, P.; He, C.; Qiu, X.; Liu, A.; Chen, L.; Chen, X.; Jing, X. *Biomaterials* **2005**, *26*, 6296−6304.